Coastal Oyster Aquaculture Area Extraction and Nutrient Loading Estimation Using a GF-2 Satellite Image

Xiaoyu Zhang, Shuchang Ma, Cheng Su, Yongheng Shang, Tinggang Wang, and Jianwei Yin

***Abstract*—The accurate extraction of an aquaculture area is significant in aquaculture management, post-disaster evaluation, and aquatic environment protection. However, little attention has been paid to the aquaculture area extraction in coastal water with high turbidity. In this study, based on the spectral and geospatial features of aquaculture cages in complex coastal water with varying turbidity, we proposed a new aquaculture area extraction method using a Gaofen-2 (GF-2) satellite image with 0.8-m spatial resolution. The water was classified into clear, medium, and high turbidity categories according to the suspended sediment concentration derived from the inversion of the GF-2 image. Different rules of extraction were developed with respect to those three categories of water body: First, the normalized difference water index threshold was set for the clear water, second, a ratio index (R = Green/NIR) was established for the medium turbid water body, and third, for the turbid water body, feature analysis with a specified classification rule was established. The experimental results demonstrated that our proposed method worked well, with the high accuracies of 87.3300% for the overall accuracy, even for the high turbidity water. The kappa coefficient was 0.7375, which was much better than the kappa coefficient values of the three conventional classification methods represented in this article. This study provides effective information support and auxiliary decision analysis for management departments to scientifically plan and environmentally manage coastal aquaculture areas.**

***Index Terms*—A new aquaculture area extraction methods, coastal aquaculture, complex water body, conventional classification method, nutrients loading estimation.**

Manuscript received November 29, 2019; revised March 18, 2020 and May 19, 2020; accepted July 31, 2020. Date of publication August 24, 2020; date of current version September 7, 2020. This work was supported in part by the National Key Research and Development Program of China under Grant 2018YFC1406604 and Grant 2016YFC1400903, in part by the National Natural Science Foundation of China under Grant 61825205 and Grant 61772459, in part by the National Science and Technology Major Project of China (50-D36B02-9002-16/19), and in part by the Zhejiang Provincial Natural Science Foundation of China (Y17D010019). *(Corresponding author: Xiaoyu Zhang.)*

Xiaoyu Zhang is with the School of Earth Sciences, Zhejiang University, Hangzhou 310027, China, with the Key Laboratory of Zhejiang Ocean Observation-Imaging Testbed of Zhejiang Province, Zhoushan 316000, China, and also with the Ocean Academy, Zhejiang University, Zhoushan 316000, China (e-mail: zhang_xiaoyu@zju.edu.cn).

Shuchang Ma, Cheng Su, and Tinggang Wang are with the School of Earth Sciences, Zhejiang University, Hangzhou 310027, China (e-mail: 18787189707@163.com; sc20184@zju.edu.cn; 565937066@qq.com).

Yongheng Shang and Jianwei Yin are with the Engineering Center of High Resolution Earth Observation, Zhejiang University, Hangzhou 310027, China (e-mail: yh_shang@zju.edu.cn; zjuyjw@cs.zju.edu.cn).

Digital Object Identifier 10.1109/JSTARS.2020.3016823

I. Introduction

AQUACULTURE is an important guarantee for world food security. In 2016, aquaculture accounted for 53% of total global fish production, whereas China's aquaculture accounted for 73.7% of the country's total fish production [1]. With the rapid development of the offshore aquaculture industry, the accurate extraction of aquaculture areas has gained great significance for offshore fishery culture activity monitoring, production estimation, food security assessment, seawater quality assessment, sustainable ecological development evaluation, disaster assessment, and postdisaster rescue [2]. However, traditional on-site investigation is laborious and time consuming with low efficiency. The development of innovative methods with high accuracy and efficiency is urgent in the fields of aquaculture area identification and extraction. High spatial resolution satellites with submeter resolution have been one of the powerful means for the dynamic monitoring of aquaculture. They have the advantages of the high accuracy of spatial expression, near real-time operation, low cost, rapid revisit, and wide coverage. However, the special land–sea interaction environment in China's offshore waters makes China's offshore water bodies exhibit high dynamic turbidity with drastic dynamic changes, which are constantly changing in space and time, making traditional image processing methods difficult to be effective. Therefore, it is necessary to develop construction of accurate recognition algorithm for aquaculture target under complex water body.

Methods for extracting marine aquaculture from satellite images have been previously developed, including visual interpretation [3], correspondence analysis [4], ratio index analysis [5], information extraction based on spatial structure analysis [6], deep learning [7], spatial spectral unmixing [8], Bayesian decision theory [9], and object-based information extraction[10], and their performances have been evaluated [11]–[13]. Among these methods, visual interpretation is simple and easy to use, but the interpretation results are generally impacted by the professional knowledge and interpretation experience of the interpreters, and it is difficult for the interpreters to discern an aquaculture area from a nonaquaculture area when the areas exhibit similar spectral characteristics or spatial structure characteristics. Correspondence analysis is extremely stringent in terms of the quality of remote sensing images. Moreover, it has no efficient solutions to the traditional classification problem

of the "same spectrum of foreign body." Ratio index analysis works well only for breeding areas that show obvious spectrum differences from the background because it considers only the grayscale information of each band. Furthermore, the "salt and pepper" problem that is common in traditional remote sensing classification impairs its effect greatly. Deep learning has strong advantages in terms of targets classification and recognition [14], and it is a promising method in satellite remote sensing [15]. However, the requirement of massive satellite images with high resolution limits its wide application in aquaculture area extraction. The spatial–spectral unmixing method is mainly based on the difference in reflectance between different objects, but the occurrence of the "same spectrum of foreign body" and the "same body of foreign spectrum" greatly interfere with its effects [8]. Classification using Bayesian decision theory requires strict sample points. Insufficient or unrepresentative training samples for the discrete probability density of sample points cause classification confusion [9]. In contrast, object-based image analysis breaks through the limitations of the traditional methods that treat a pixel as the basic classification and processing unit. This method exhibits improved capability in reflecting the multiscale and multifeature characteristics of the groundlike patches in a sea area, and it is closer to the human understanding of real-world features [10]. Additionally, it combines the features of surface spectrum, spatial geometry, shape, texture, etc., which are very helpful in improving classification accuracy [16], [17].

At present, few studies have been carried out on the extraction of aquaculture areas for complex coastal water with varying turbidity. Turbid coastal water exhibits similar spectral features to target objectives with strong reflectance, which causes the phenomenon of the "same spectrum of foreign body" in an aquaculture area [18]. Additionally, with the improved capability in recognizing subtle features, the phenomena of "salt and pepper" [19] and the "same body of foreign spectrum" occur frequently when processing satellite images with high spatial resolutions [20]. Therefore, determining how to accurately extract an aquaculture area in turbid waters is a huge challenge. In principle, aquaculture area extraction involves the extraction of target objects from a water body. Identifying and removing the water body is the first step of the process. For clean water, the reflectivity of water is much weaker than that of other target objects, and it decreases obviously with the increasing wavelength. Target objectives can be accurately identified and extracted from the surrounding water according to the spectral characteristics [21]. However, due to the high turbidity of coastal waters, the traditional method of recognizing and separating targets from seawater as the first step is no longer feasible. Some conventional methods, such as visual interpretation, correspondence analysis, and ratio index analysis, are inefficient in this case. Similarly, due to the weak generalization of features, it is difficult to obtain satisfactory accuracy using deep learning. The determination of how to extract aquaculture areas with acceptable accuracy in turbid waters needs to be reconsidered. The situation becomes more complicated when the breeding area contains varying turbid waters.

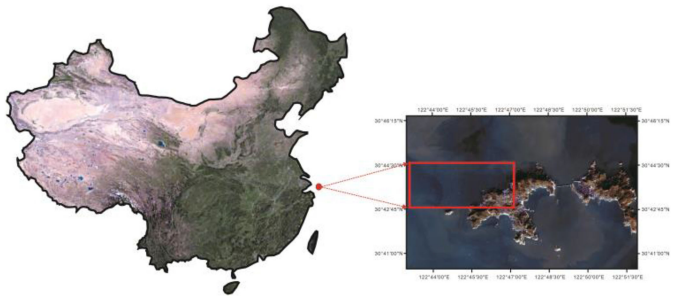

Fig. 1. Schematic map of the study area.

The Changjiang (Yangtze) Estuary in China is one of the most turbid areas in the world. It is characterized by very high suspended sediment concentration (SSC) and dynamic spatial variation. Additionally, Changjiang Estuary is one of the most productive aquacultures in China. In view of this, we took the oyster aquaculture area in Gouqi Island, Zhoushan (it is located at the mouth of the Changjiang Estuary) as the test area (see Fig. 1). A Gaofen-2 (GF-2) satellite image with 0.8-m spatial resolution is employed in this study. A set of general rules applicable to waters with different turbidities based on an object-based extraction method was developed. In order to improve the extraction accuracy, we classified the water into three categories according to the turbidity. The thresholds of turbidity were determined by the SSC inverted from the same satellite image. The extraction accuracy of this method was compared with the maximum likelihood, neural network, and support vector machine (SVM) methods that are widely used in remote sensing. The aquaculture area that was extracted with the best method was used to estimate the nutrient content through aquaculture activities. The ubiquitous applicability of the threshold values of the turbidity and the rules determined for each category of water body proposed in this study will be discussed elsewhere.

II. Study Area

The study area was located on the western coast of Gouqi Island, Zhoushan, China (see Fig. 1), with the geographical position of 122°43′–122°46′E and 30°42′–30°44′N. The convergence of fresh Changjiang River diluted water with saline seawater and upwelling stimulates the high primary production in this area, which fosters the Zhoushan fishery as one of the biggest fisheries in the world. Zhoushan is also one of the most productive aquacultures in China with plentiful breeding species, and the mussel production is about 85 000 ton/a. However, due to the complex hydrodynamics, the seawater in this area is temporally and spatially dynamically variable from highly turbid to clean, which poses a great challenge for the efficient monitoring of the aquaculture area by satellite remote sensing. In addition, the Zhoushan sea area is endangered, with frequent occurrences of red tides, oil spills, and typhoons. The accurate real-time observation of aquaculture is the basis for accomplishing efficient early warnings and postdisaster rescues. Furthermore, the evaluation of the nutrients input by aquaculture

TABLE I
TECHNICAL PARAMETERS OF THE TWO DIFFERENT LOADINGS ON THE GF-2 SATELLITE

Satellite parameters		GF-2	GF-1	WorldView-2
Spatial resolution/m	Panchromatic	0.8	2	0.46
	Multispectral	3.2	8	1.84
Coastal blue(C) /μm		-	-	0.4-0.45
Blue(B) /μm		0.45-0.52 (B1)	0.45-0.52 (B1)	0.45-0.51
Green(G) /μm		0.52-0.59 (B2)	0.52-0.59 (B2)	0.51-0.58
Yellow(Y) /μm		-	-	0.585-0.625
Red(R) /μm		0.63-0.69 (B3)	0.63-0.69 (B3)	0.63-0.69
Red edge(RE) /μm		-	-	0.705-0.745
Near Infrared 1(NIR1)/μm		0.77-0.89 (B4)	0.77-0.89 (B4)	0.77-0.895
Near Infrared 2(NIR2)/μm		-	-	0.86-1.04

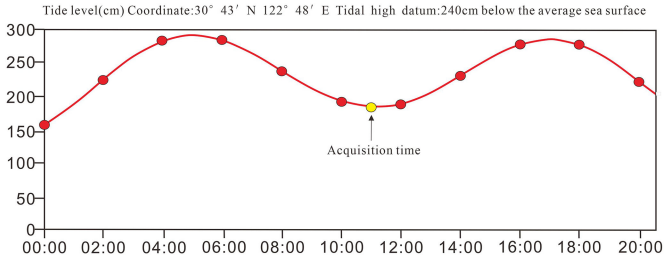

Fig. 2. Tidal prediction table on January 16, 2016 (Note: the yellow dot represents the time at which the GF-2 satellite images were captured).

is important for the coastal aqua environment management of the serious eutrophication this area is facing.

III. SATELLITE DATA

The GF-2 satellite is a civilian optical satellite of China. It is equipped with two sets of multispectral and panchromatic cameras. The coverage width is 45 km with revisit period of 5 days, and the coverage period is 69 days. The band design and the related technical parameters of the GF-2 in comparison with Worldview-2 and GF-1 are listed in Table I. Worldview-2 is currently one of the satellites with the most abundant information, and its diverse spectrum provides users with the ability to perform accurate change detection and mapping. GF-2 is similar to the Worldview-2 satellite in terms of its spectrum settings, which are of great significance for improving the self-sufficiency rate of high-resolution earth observation data in China and achieving high spatial resolution with a quick revisit. As a sequential sister satellite, GF-2 is identical to GF-1 in terms of its band parameter settings. We transplanted the SSC inversion algorithm from GF-1 to obtain the SSC for GF-2 in this study. It is noteworthy that the apparent reflectance data for the two satellites were highly consistent [22].

A GF-2 satellite image taken at 11:00 local time on January 16, 2016 was employed in this study. The image was selected because it was taken during the low tide of the ebb tide when most of the cages stuck out of the turbid water and were visible to the greatest extent (see Fig. 2). In particular, the SSC was relatively low [23], [24].

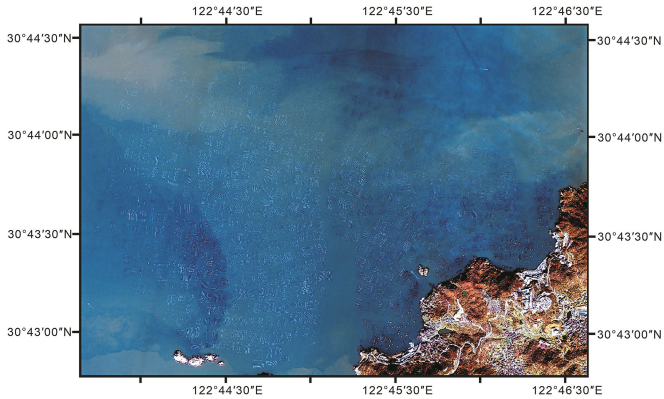

Fig. 3. False-color synthesized map of the study area (GF-2, 3-2-1, RGB band synthesis).

IV. METHODS

As shown in Fig. 3, the cages were arranged in a disorderly manner in some areas, showing irregular polygon texture or even messes in the satellite image. It is notable that for the high turbidity, the cages were difficult to discern from the surrounding water in the satellite image. Moreover, the aquaculture areas exhibited similar spectral characteristics to the base rocks of the island, which resulted in the misclassification of cages into land. In view of this, the spectral characteristics of the target objects and the surrounding water needed to be examined before we constructed the extraction method. We selected water bodies with different turbidities and cages in waters with different turbidities and land for the spectral reflectance calculation with the GF-2 satellite data. The sampling points are shown in Fig. 4.

It was noted that apart from the land, the all other five types of objects exhibited similar spectral features. Specially, all the objects had a similar spectral reflectance pattern in the blue and green bands, which caused difficulties in identifying and extracting targets with spectral characteristics alone. However, subtle differences of the spectral reflectance were observed with increasing bands, and the spectral reflectivity and corresponding spectral index could be used to identify and extract the aquaculture area from the surrounding waters. It was noted that the accuracy was low in very turbid waters only if the spectral information was used due to problems, such as the "same spectrum of foreign body," the "same body of foreign spectrum," and "salt and pepper." Therefore, using one rule for all regions may have been inappropriate. Based on the aforementioned analysis, it was suggested that an appropriate extraction method should be constructed for different categories of waters according to the turbidity in order to improve the extraction accuracy; specifically, for highly turbid waters, a set of rules relating to the features of spectrum, shape, and texture should be established.

Before the experiment, the GF-2 satellite image was preprocessed by image clipping, orthocorrection, radiometric calibration, and atmospheric correction. Image fusion was also performed for the subsequent experimental analysis. The experimental environment CPU was an Intel (R) Core (TM) i5-5200U,

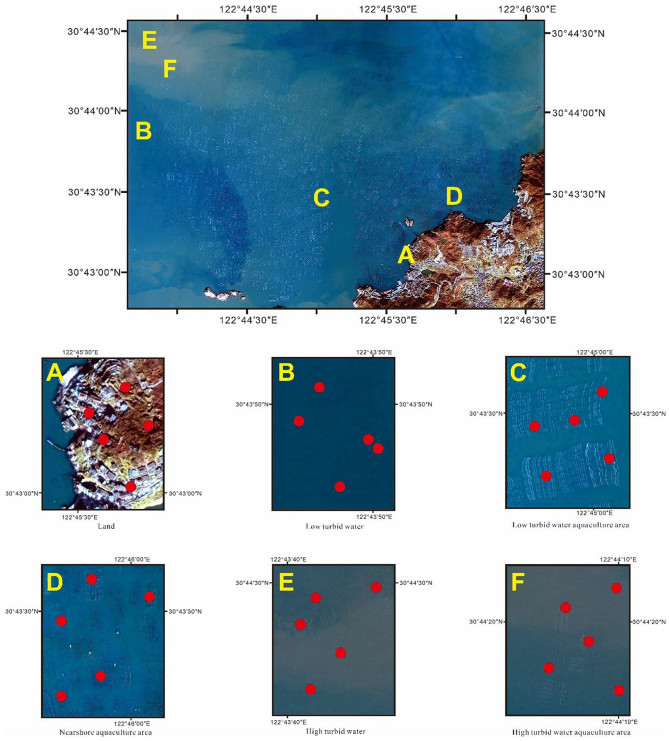

Fig. 4. Sampling points of the six typical objects in the satellite image.

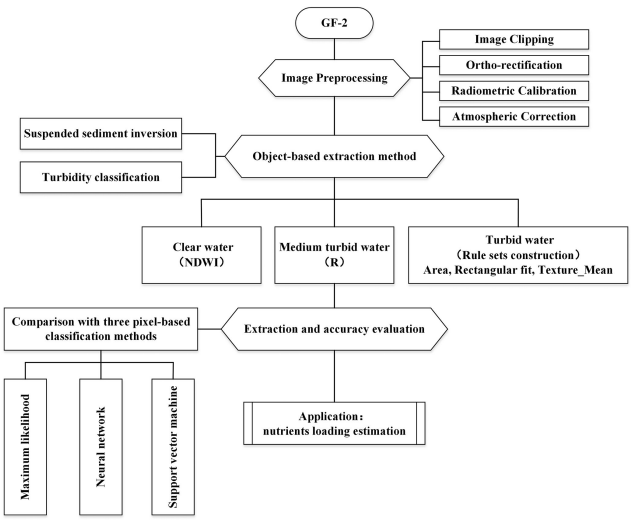

Fig. 5. Technology roadmap utilized in this study.

2.20 GHz, 8-GB memory PC. The experiment was performed using the commercial software programs Envi 5.3, e-Cognition 9.2, and ArcGIS 10.2. The road map adopted in this study is shown in Fig. 5.

A. SSC Inversion and Turbidity Categories Classification

The turbidity of the seawater was graded according to the inversed SSC with the GF-2 satellite data. An SSC inversion model developed for the Zhoushan sea area with GF-1 [25] was adopted. Considering the high consistency of GF-1 and GF-2

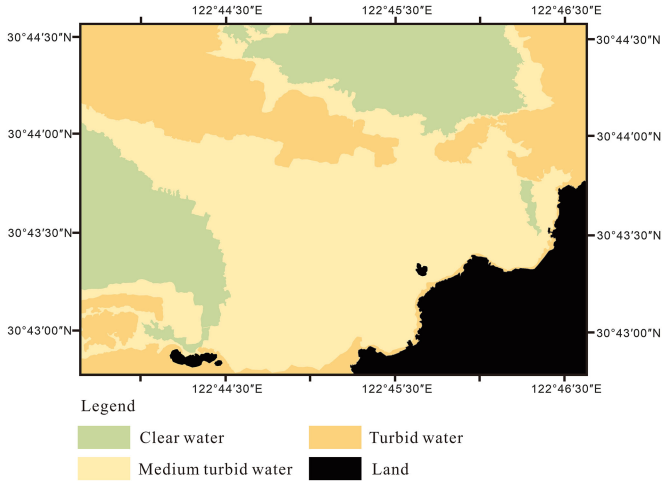

Fig. 6. Results for suspended sediments inversion.

in the band design, the transplant of the GF-1 SSC inversion model for the GF-2 data was indicated to be acceptable. The formulation of the inversion algorithm is illustrated as

$$\mathrm{SSC} = 1.4856 \times (\mathrm{B3}/\mathrm{B2}) - 1.1129. \quad (1)$$

In the formula, B3 and B2 are the reflectances of the red and green bands, respectively. The inversion results are shown in Fig. 6. The inversion SSC conformed to previous studies in this area [26], [27].

The seawater was classified into three categories according to the inversed SSC: clear water with an SSC between 0–0.33 g/L, medium turbid water with an SSC of 0.33–0.46 g/L, and turbid water with an SSC higher than 0.46 g/L. The corresponding rules were constructed under different turbidities, which led to the improvement of the object extraction accuracy and efficiency.

B. Aquaculture Area Extraction Rules

The aquaculture in waters with various turbidities exhibited distinguished spectral or texture features (see Fig. 6). It is noteworthy that most of the cages were located in medium or high turbidity waters, which blurred the boundaries and texture of the aquaculture area. The followings are a set of extraction rules for aquaculture areas in water bodies with different turbidities.

1) Clear Water: In clear water, the boundary and texture of each cage were clearly visible. The normalized water body index (NDWI), utilizing the differences between the absorption and reflection characteristics of the near-infrared band and the green band [28], was employed to extract the aquaculture cages in this study. The NDWI extraction threshold was repeatedly adjusted and it was finally determined to be 0.221.

2) Medium Turbidity Water: In medium turbidity waters, the visibility of the raft was greatly affected by the SSC. Only a few strips and blurred outlines of the cages could be identified, and no clear edges between the water body and the cage were observed. Therefore, a characteristic index with a spectral ratio was employed to enhance the accuracy of the aquaculture area extraction.

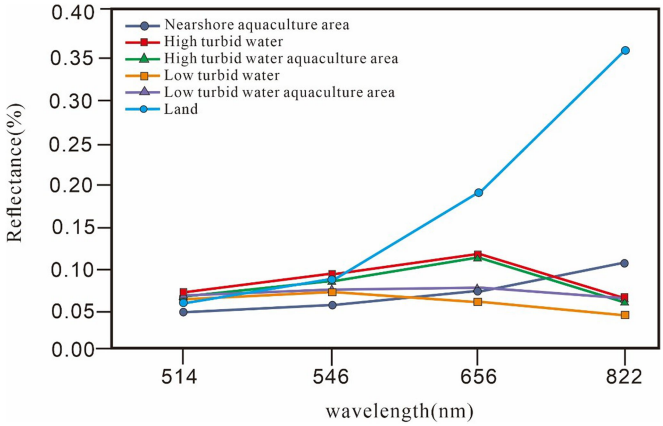

Fig. 7. Spectral reflectance of the six types of objects in this study.

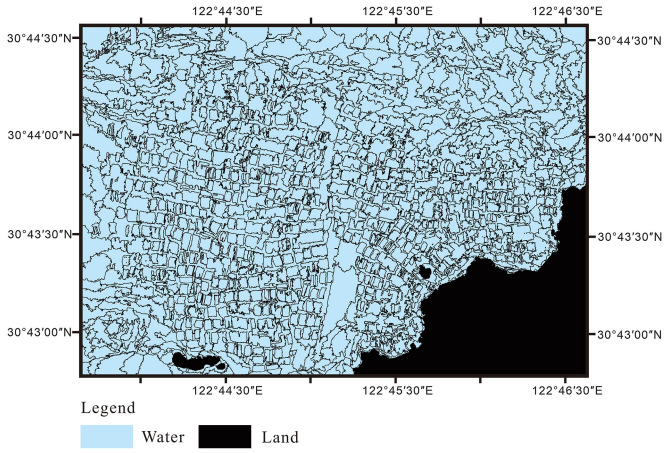

Fig. 8. Segmentation effect.

TABLE II
RULE-BASED CLASSIFICATION RULES

Aquaculture area	Rules
Clear water	NDWI≤0.221
Medium turbid water	R≤1.541
	1500pxl≤Area≤10800pxl
Turbid water	Rectangular fit>0.6
	85≤Texture_Mean≤110

Based on the spectral features of the cages in the medium turbidity water (see Fig. 7) and the ratio index constructed in previous studies [29], [30], the green and near infrared bands were selected to establish a ratio index [illustrated as formula (2)]. The index highlighted the target objects and effectively reduced the interference from the background turbid water [29]

$$R = \mathrm{B2}/\mathrm{B4}. \tag{2}$$

In this formula, R is the ratio index and B2 and B4 are the reflectance of the green band and the near-infrared band, respectively. The threshold value of R was determined to be 1.541.

3) High Turbidity Water: In the water with high turbidity, the culture area was almost invisible in the GF-2 satellite image. The differences between the turbid water and the aquaculture area were so small that it was impossible to extract the cages from the water with the NDWI or the ratio index (R). Therefore, rules were established based on the shape, texture, and spectral information, as shown in Table II.

C. Segmentation

Before applying the rules to extract the aquaculture, image segmentation needed to be performed. The image was segmented into various regions based on certain features. Images that had similar attributes were in the same region, and vice versa [31]. In this study, the feature extraction (FX) module of Envi was used to perform multiscale segmentation. The FX module adopted the image edge block calculation method based on the brightness, texture, and color characteristics of neighboring pixels. The segmentation was performed by setting the scale parameters that varied from 0–100. The determination of the segmentation value was extremely important. A higher scale level resulted in fewer patches. The merging was used to recalculate the result of the segmentation, and to prevent the same object from being divided into multiple patches. The merge lever also varied from 0–100. The larger the merge level was, the smaller the number of patches that were produced by the segmentation; that is, the internal consistency of the resulting object was poor.

Generally, the selections of the segmentation and merge levels were related to the scale of the target features, which determined the maximum allowed heterogeneity for the objects [32]. At the beginning of the experiment, the medium-scale level (i.e., 50) was set as a reference. Because the extraction of the aquaculture area was more complex than that of water, the optimal scale levels were tested in the range of 50–100. The merge level was slightly larger than the corresponding scale level. The scale level and the merge level were tested by dichotomy up to 100 [33]. Finally, the scale level was set to 65, the merge level was set to 70, and the texture kernel size defaulted to 3. The result is shown in Fig. 8.

D. Aquaculture Area Extraction

Fig. 9 shows the extraction result of the aquaculture areas using the aforementioned extraction method with consideration of the different turbidities. The extraction effect of the target object was visually acceptable, especially in the nearshore area with a high bottom reflectance and in the sea areas with high turbidity. The irregular shape of a small part of the culture areas was caused by partial immersion with turbid water.

The Create Random Points tool in ArcGIS software was also utilized to quantitatively evaluate the extraction results objectively. In total, 300 points were generated in the study area. By visually interpreting the actual category of each point, 176 points were identified as the aquaculture areas, of which

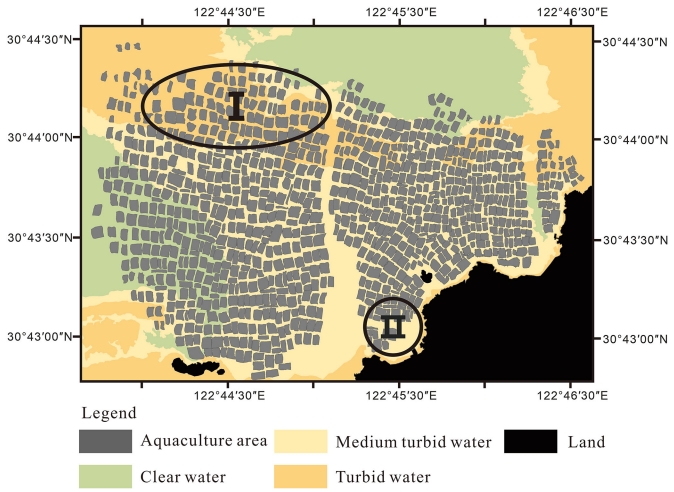

Fig. 9. New classification method results.

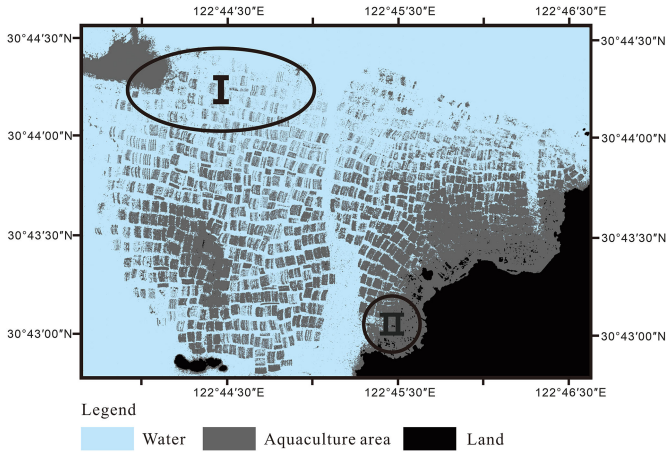

Fig. 10. Maximum likelihood classification results.

159 points were correctly extracted, 17 points were missed, and 21 points were misclassified. It is calculated that the overall accuracy of extracting aquaculture area is 87.3300%, and the kappa coefficient is 0.7375.

V. Comparison With Conventional Classification Methods

Three conventional classification methods of a maximum likelihood method, a neural network, and a SVM algorithm were selected in this study for comparative experiments. The SVM adopted the principle of structural risk minimization, and the maximum likelihood used a Bayesian discriminant criterion, whereas the neural network adopted an iterative algorithm. These three classifiers are widely used in object classifications; e.g., land cover, because of their superior performance [34]–[36].

Before performing the classification, training samples are selected in Envi with the following criteria: first, the regional category of the pixels in the training samples needed to have the same type of features. Second, the selected sample pixels had to be representative [36]. When weighing the classification accuracy and the workload, the optimal number of training samples was 20 for each category [37]. Therefore, a total of 20 aquaculture area samples containing 34 125 pixels and 20 water samples containing 19 883 pixels were selected. It was found that the separability between aquaculture area and water samples reached 1.8228 by checking the quality of samples, which were qualified samples for the experiment of extracting aquaculture area by three conventional methods.

A. Maximum Likelihood Method

When we performed the classification with the maximum likelihood method, the likelihood threshold was set to 0.001 for all of the training samples. The classification results are shown in Fig. 10. The classification results were less than ideal, especially for the aquaculture areas in high turbidity waters (see region I in Fig. 10) and the nearshore water bodies of the shoal (see region II in Fig. 10). The maximum likelihood method was used to establish discriminant functions for the evaluation of the similarity between the other pixels and training categories based on the training samples. Because of the highly turbid water in the study area, the training samples had no distinguished spectral characteristics, which led to low accuracy and a poor effect. The classification of the aquaculture areas in region II was clearly a misclassification, which may have been due to the strong bottom reflectance of the shallow depth of the shoal.

Accuracy evaluation is very important for remote sensing image classification, it represents the feasibility of classification methods. This article uses the most commonly used confusion matrix method to evaluate the classification accuracy. The overall accuracy represents the probability that all the correctly classified samples account for the total number of samples, which can reflect the overall accuracy of the classification results; the kappa coefficient is the accuracy coefficient that represents the overall classification, usually the K value range is between 0–1, When $K = 1$, it means that the classification result is completely consistent with the actual type. The larger the K value, the higher the classification result and the actual type, and the higher the classification accuracy. When the K value is less than 0.4, it indicates that the degree of consistency is not ideal; when the K value is between 0.40 and 0.75, it indicates that the two are in general agreement; when the K value is greater than 0.75, it indicates that both are in good consistency.

Select the accuracy verification sample on the GF-2 original image used in the experiment. The verification sample selection principle is similar to the training sample selection principle, and the authenticity of the obtained category reference source must be guaranteed. A total of 26 413 pixels of aquaculture area verification samples and 26 110 pixels of water area verification samples were selected. The results were shown in Table III. The overall accuracy of the maximum likelihood method was 85.1951%, and the kappa coefficient was 0.7042.

B. Neural Network

The training root mean square (rms) exit criteria parameter was the root of the classification accuracy. A smaller rms indicated fewer output results with higher accuracy, and vice

TABLE III
EVALUATION OF CLASSIFICATION RESULTS OF MAXIMUM LIKELIHOOD METHOD

Class	Prodcucer Accuracy /%	User Accuracy/%	Prodcucer Accuracy(Pixels)	User Accuracy(Pixels)
Aquaculture areas	75.72	93.62	19999/26413	19999/21361
Water	94.79	79.42	24748/26110	24748/31160
Overall Accuracy/%			85.1951	
Kappa Coefficient			0.7042	

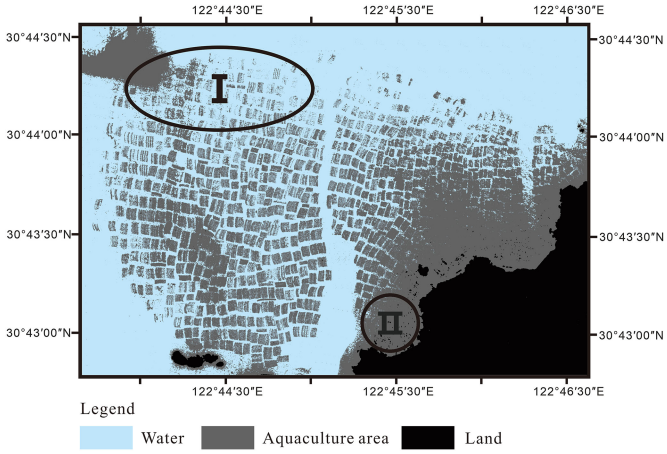

Fig. 11. Neural network classification results.

TABLE IV
EVALUATION OF CLASSIFICATION RESULTS OF NEURAL NETWORK METHOD

Class	Prodcucer Accuracy /%	User Accuracy/%	Prodcucer Accuracy(Pixels)	User Accuracy(Pixels)
Aquaculture areas	77.31	90.69	20419/26413	20419/22515
Water	91.97	80.03	24014/26110	24014/30008
Overall Accuracy/%			84.5972	
Kappa Coefficient			0.6922	

versa. The rms needed to be tested repeatedly at the expense of the classification efficiency [38]. After repeated adjustment, the rms was set to 0.1 and the number of iterations was set to 2000 in this study.

The classification results of the neural network (see Fig. 11) were similar to those of the maximum likelihood method, but its capability in discriminating between the aquaculture area and the water was poorer, and the texture of the aquaculture area in some areas was more sparse and obscured. It was indicated that the neural network classification method was based on pixels, and the context relationships between the pixels and their adjacent pixels were not fully considered, so it was difficult to correctly extract breeding areas with large regional heterogeneity.

The accuracy evaluation of the classification results of the neural network was shown in Table IV. The overall accuracy of the maximum likelihood method was 84.5972%, and the kappa coefficient was 0.6922.

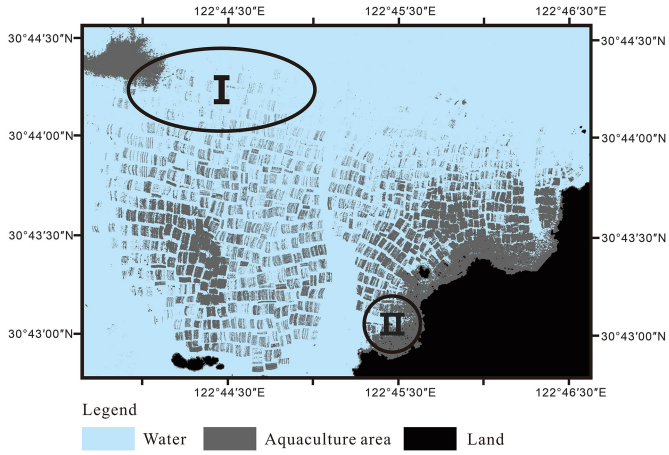

Fig. 12. SVM classification results.

TABLE V
EVALUATION OF CLASSIFICATION RESULTS OF SVM METHOD

Class	Prodcucer Accuracy /%	User Accuracy/%	Prodcucer Accuracy(Pixels)	User Accuracy(Pixels)
Aquaculture areas	53.78	97.61	14205/26413	14205/14553
Water	98.67	67.85	25762/26110	25762/37970
Overall Accuracy/%			76.0943	
Kappa Coefficient			0.5231	

C. Support Vector Machine

The classification effect of SVMs is affected by the selection of the kernel type. Therefore, appropriate kernel function and parameters are very important for achieving the optimal extraction effect. With sufficient training samples and empirical data, the classification accuracy of the polynomial classifier is the highest, as well as the overall classification accuracy and kappa coefficient, and the classification effect is better than that of other classifiers [39]. Therefore, we chose a polynomial as the kernel type for SVM classification in this study. The number of polynomials was set to six after multiple adjustments.

The SVM classification results (see Fig. 12) were somewhat different from the results of the other two methods. The SVM performed well in distinguishing aquaculture areas nearshore where the bottom reflectance was high. However, the aquaculture area was poorly identified in the northwest with high turbidity. The imbalance of the training samples in the SVM classification may have been what affected the results. In the study area, the features of the different types of cages were unevenly distributed in the characteristic space. This induced extreme imbalance in the waters with different turbidities, which impaired the classification results by the SVM.

The accuracy evaluation of the classification results of the SVM was shown in Table V. The overall accuracy of the maximum likelihood method was 76.0943%, and the kappa coefficient was 0.5231.

TABLE VI
ACCURACY COMPARISON OF VARIOUS METHODS

Extraction method	The new classification method	conventional classification		
		Maximum likelihood	Neural network	Support vector machine
Kappa	0.7375	0.7042	0.6922	0.5231
Overall Accuracy/%	87.3300	85.1951	84.5972	76.0943

D. Comparisons

According to the summary of the extraction accuracy of each method in Table VI, it can be seen that the accuracy and kappa coefficient of the new extraction method are the highest, which shows that the new method could avoid the drawbacks of the single extraction rule and achieve efficient and accurate extraction results via a set of rules for various water bodies with different turbidities. In contrast, the conventional classification methods exhibited poor performance, especially for the high turbidity seawater and the shoal.

Among the three conventional methods, the maximum likelihood method had the highest overall accuracy and kappa coefficient, whereas the SVM had the lowest overall accuracy and kappa coefficient. The classification results of the maximum likelihood method in high turbid region I were fragmented, and only the part with very high spectral reflectance could be extracted. The sea area with high turbidity was wrongly classified as the aquaculture area, as well as the other two areas (see Figs. 11 and 12). In general, the three conventional classification methods were likely to cause spatial data redundancy and low classification accuracy. The spatial characteristics of the image and the topological relationships of the objects were ignored and only the spectral information was considered, which made the qualitative analysis of the graphics processing difficult. In contrast, the method we proposed worked well in this case, and the water channel between the cages was clearly identified (see Fig. 9).

Moreover, all three of the conventional extraction methods misclassified the shoal as aquaculture areas (see Figs. 10–12). It is noteworthy that when the extraction method we proposed started to extract targets using the spectral texture features, it performed the image segmentation first. In this case, the extracted object was a collection of similar pixels, which avoided "salt and pepper noise" (see Fig. 9). This was the same reason that a "gray edge" occurred in all three of the conventional classification results along the coast of island, rather than in the results for the method proposed in this study. The appearance of the "gray edge" may have been due to the high bottom reflectivity of the shoal around the island. Because of the different basic units of classification, the postclassification process of the method proposed in this study could easily handle this holistic misclassification problem, whereas the traditional methods of postclassification could only remove some small noise and misclassification, and no effective solution was available to deal with a "gray edge."

In summary, to achieve a better extraction effect for the aquaculture in this area, the impacts from the waters with different turbidity had to be taken into account. However, the three conventional classification methods failed in this case because of their ignorance of the varying turbid water body as background. Therefore, the introduction of spectral features and features, such as the shape, area, and texture, was indicated to be beneficial for the extraction when we constructed the feature index and the rule set for the segmentation and extraction in this study.

However, there were still some factors that affected the extraction accuracy. First, in principle, the classification of the membership function itself was based on fuzzy set theory. There was uncertainty in the determination of the classification rules and the thresholds under each rule. Second, the disordered layout of the cages or rafts induced chaotic spectral reflection and mixed pixels, which may have affected the effects of image segmentation and subsequent classification. Additionally, the immersion of the cages in the water led to the spectral homogenization of the aquaculture and background, which impaired the extraction accuracy. These factors explained the irregular patches in the aquaculture extraction results. It is noteworthy that the problem of the aquaculture area itself was present in any classification extraction method. In addition, the turbidity affected the classification accuracy. Although the extraction methods proposed in this study worked effectively for the middle and high turbidity water, the very high turbidity had an inevitable impact on the extraction accuracy due to its similar spectral features to the land. Furthermore, the cost of the run time of the extraction method we proposed was accepted to be much faster (476 s) than the neural network (2580 s), but it was a little slower than the SVM (63 s) and the maximum likelihood method (20 s).

VI. EXPERIMENTAL VERIFICATION

In order to further verify the reliability and generalizability of the aquaculture area extraction method proposed in this article, we selected GF-2 images of three representative regions for verification: aquaculture area with uniformly clear water; the same aquaculture area in Gouqi Island but imaged at different time; and different aquaculture area containing varying turbid water.

A. Aquaculture Area in Uniformly Clear Water

It is noteworthy that selecting aquaculture areas with uniformly clean water is not easy because most of the coastal aquaculture areas are distributed in areas with varying turbid water. The situation highlights the significance of this article to propose method for accurate identification of aquaculture areas under complex water. Therefore, a small piece of aquaculture area distributed in clear water from a GF-2 image (taken on December 21, 2017) of Fujian's offshore aquaculture area was tailored for comparative experiments as a compromise.

The accuracy test results are shown in Fig. 13 and Table VII. It can be seen that in the area of simple water environment, both the extraction accuracy and reliability of various methods are very high, indicating that most methods perform well for aquaculture area with uniformly clean water.

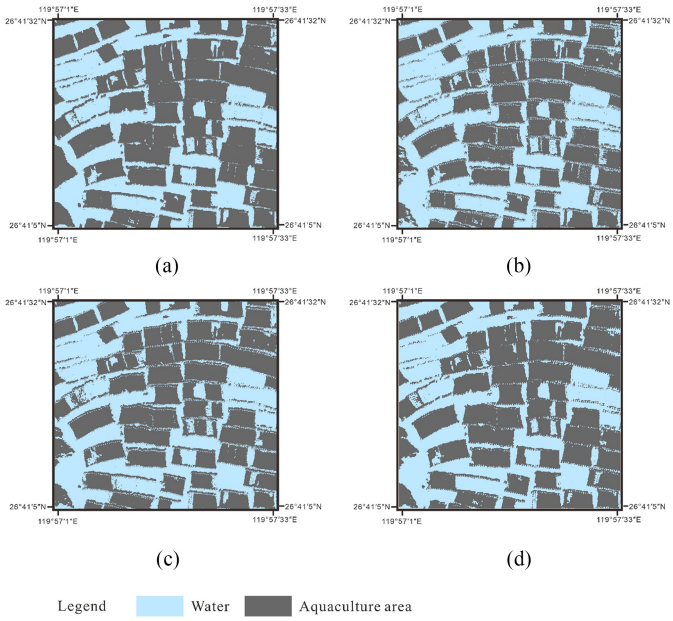

Fig. 13. Extraction results of different methods in clear water aquaculture area. (a) New method. (b) Neural network method. (c) Support vector machine method. (d) Maximum likelihood method.

TABLE VII
COMPARISON OF EXTRACTION ACCURACY OF DIFFERENT METHODS IN UNIFORMLY CLEAR WATER

Method	Overall Accuracy/%	Kappa Coefficient
New method	92.0000	0.8321
Neural Network method	91.5600	0.8305
Support Vector Machine method	91.8142	0.8367
Maximum likelihood method	92.2494	0.8446

B. Sea Area Around Gouqi Island in Different Time

Even though the GF-2 image of the same aquaculture area near the Gouqi Island was taken on February 3, 2019, different time from the previous one, the water are still highly varying turbid, indicating that the aquaculture area is usually under a turbulent water environment.

The experimental results are shown in Fig. 14 and Table VIII. It can be seen that the extraction method proposed in this article still shows obvious advantages in this case with the highest extraction accuracy and kappa coefficient. In contrary, the traditional three extraction methods of aquaculture areas are not good at identifying aquaculture areas from turbid waters with low accuracy of extraction.

C. Complex Water With Varying Turbidity in Fujian Offshore

The aquaculture species in the coastal areas of Fujian Province are diverse and unevenly distributed, exhibiting different shape and texture of seafood farming rafts.

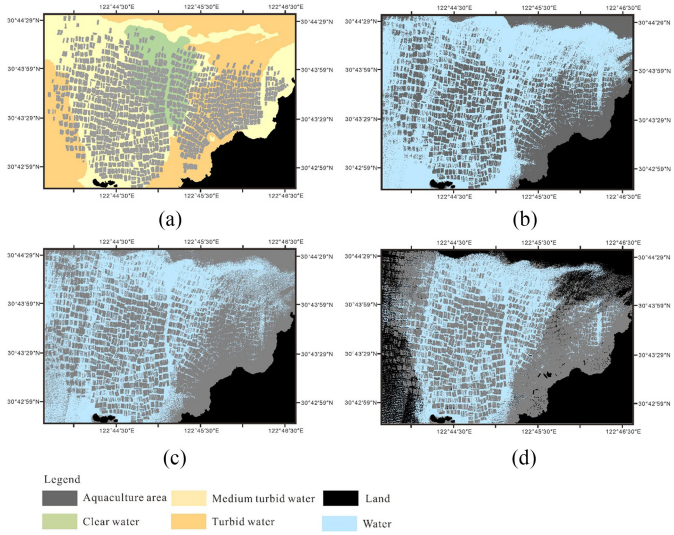

Fig. 14. Extraction results of different methods in complex water background (Gouqi Island). (a) New method. (b) Neural network method. (c) Support vector machine method. (d) Maximum likelihood method.

TABLE VIII
COMPARISON OF EXTRACTION ACCURACY OF DIFFERENT METHODS IN SEA AREA AROUND GOUQI ISLAN

Method	Overall Accuracy/%	Kappa Coefficient
New method	89.0000	0.7792
Neural Network method	88.6896	0.7749
Support Vector Machine method	86.8026	0.7330
Maximum likelihood method	77.6928	0.5890

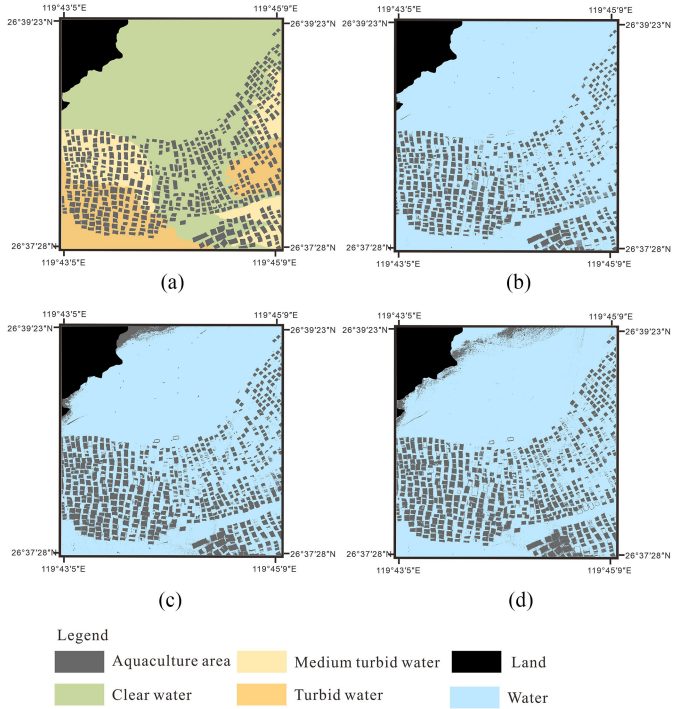

Fig. 15. Extraction results of different methods in complex water background (Fujian offshore). (a) New method. (b) Neural network method. (c) Support vector machine method. (d) Maximum likelihood method.

TABLE IX
COMPARISON OF EXTRACTION ACCURACY OF DIFFERENT METHODS IN FUJIAN OFFSHORE

Method	Overall Accuracy/%	Kappa Coefficient
New method	92.5000	0.8337
Neural Network method	87.2774	0.7465
Support Vector Machine method	93.0883	0.8620
Maximum likelihood method	93.9869	0.8803

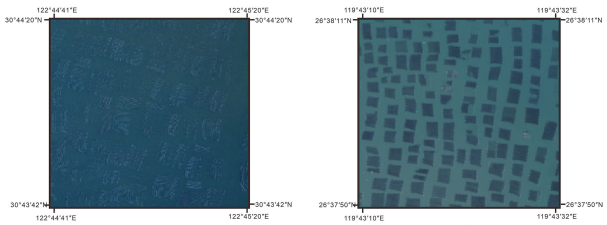

Fig. 16. Comparison of two aquaculture areas. (a) Gouqi island aquaculture area. (b) Fujian offshore aquaculture area.

The experimental results are shown in Fig. 15 and Table IX. The extraction accuracy of each method is acceptable at a relatively high level.

As shown in Fig. 16, all the methods perform better for the aquaculture in Fujian Province than those in the Gouqi Island, which may be related to the greater difference between the farming raft and the water body in aquaculture in Fujian Province with more prominent color and shape.

The verification test indicated that all the methods works well in identifying aquaculture area in uniformly clean water, and even in turbid water if the color, shape, and texture of the farming rafts are obviously different from the surrounding water. However, it should be noted that for the aquaculture with obscured properties under complex waters with varying turbidity, the extraction method proposed in this study performs well.

VII. APPLICATION: ESTIMATION OF THE NUTRIENT LOADING INDUCED BY OYSTER CAGE AQUACULTURE

Because the nutrients input by marine aquaculture superposing on the terrestrial input nutrients carried by the runoff has been the main cause leading to the severe eutrophication in China's offshore waters, it was necessary to quantify the amount of nutrients released through aquaculture activities. The aquaculture area extracted with the method we proposed in this study was used to estimate the nutrient loading by the oyster cage aquaculture in this sea area. The total aquaculture capacity was calculated based on the average breeding density of the oyster cage aquaculture, and the nitrogen and phosphorus loading in the aquaculture area was estimated. The nutrients produced from excretion and sediment exchange were also calculated.

The nitrogen and phosphorus excretion rate and amounts for 19°C–22°C for the oysters were determined by referring to Fu [41]. The estimation equation was as follows:

$$Q = Q_1 + Q_2$$
$$Q_1 = V_1 \times 24 \times \mathrm{Ar} \times n \times S_1 \times 10^{-12}$$
$$Q_2 = V_2 \times \mathrm{Ar} \times S_2 \times 10^{-9}$$

Q: the loading amount of N and P per day(t); $Q1$: the excretion amount of N and P for the oysters per day(t); $Q2$: the nutrient loading through sediment exchange to the above seawater (t); $V1$: the excretion rate per oyster [μmol/(h·ind)]; Ar: the relative atomic mass; n: the number of oysters cultured per mu (pieces); $S1$: the area of aquaculture (mu); $V2$: the exchange rate of nutrients between the sediments and the seawater (mmol·m^{-2}·d^{-1}); and $S2$: the area of aquaculture (m^2).

Note: 1 mu = 666.67 m^2.

The nitrogen and phosphorus excretion rates of the cultured oysters and the proportion of different forms of nitrogen are shown in Tables X and XI.

TABLE X
NITROGEN AND PHOSPHORUS EXCRETION RATES FOR THE OYSTERS (μMOL/(H·IND),±SD) [40]

Items	TDN	NH_4-N	Amino-N
excretion rate	3.11	2.29	0.662
±SD	(0.5)	(0.37)	(0.109)
Items	Urea-N	TDP	DIP
excretion rate	0.075	0.161	0.134
±SD	(0.015)	(0.011)	(0.016)

TABLE XI
PERCENTAGE OF VARIOUS FORMS OF *N* IN TOTAL DISSOLVED *N* EXCRETION (%±SD) [40]

Items	NH_4-N	NO_2-N	NO_3-N	Urea-N	Amino-N	Σ
percentage	73.7	1.2	0.5	2.4	21.3	99.1
±SD	(8.2)			(0.5)	(10.5)	

According to the survey results of oyster culture in the sea area of Gouqi Island by Fu [41], the density of 180 000 oysters per mu was accepted. The oyster farming area in the northern part of Gouqi Island was calculated to be 929.66 hm^2 (about 13 944.9 mu). The nitrogen and phosphorus loads of oyster excretion in the culture area were estimated. The results are shown in Table XII.

The exchange fluxes of the nitrogen and phosphorus nutrients varies in different sea areas because the material exchange rate at the sediment-seawater interface could be disturbed by the seabed types, bioturbation, currents, and other factors. Previous studies suggested great differences for the nutrient exchange flux of the sediment-seawater interface between aquaculture and nonaquaculture areas, even with similar sediments, which suggested that aquaculture activity was one of the most important factors introducing nutrients through material exchanges with

TABLE XII
ESTIMATION OF NITROGEN AND PHOSPHORUS EXCRETION FOR THE OYSTER

Item	TDN	NH_4-N	NO_2-N	NO_3-N
Excretion per day(mg)	1.045	0.769	0.013	0.005
Daily excretion per acre(g)	188.093	138.499	2.257	0.940
Daily excretion throughout the sea area(t)	2.623	1.931	0.031	0.013
Item	Amino-N	Urea-N	TDP	DIP
Excretion per day(mg)	0.222	0.025	0.120	0.100
Daily excretion per acre(g)	40.038	4.536	21.561	17.945
Daily excretion throughout the sea area(t)	0.558	0.063	0.301	0.250

TABLE XIII
SEDIMENT-SEAWATER INTERFACE EXCHANGE RATE OF THE INORGANIC NUTRIENTS IN THE AQUACULTURE AREA ($MMOL \cdot M^{-2} \cdot D^{-1}$)

Item	NH_4-N	NO_2-N	NO_3-N	DIP(PO_4-P)
Exchange rate	0.63	0.02	-0.07	0.45

TABLE XIV
NITROGEN AND PHOSPHORUS POLLUTION LOAD CAUSED BY SEDIMENT EXCHANGE

item	NH4-N	NO2-N	NO3-N	DIP(PO4-P)
Daily exchange volume of sediments (t)	0.082	0.003	-0.009	0.130

TABLE XV
ESTIMATION OF NUTRIENT LOADING IN THE AQUACULTURE AREA (T/D)

Nutrient	TDN	DIN			TDP	DIP
		NH_4-N	NO_2-N	NO_3-N		PO_4-P
Amounts	2.698	2.013	0.034	0.004	0.431	0.380

the interaction of water and sediments. Therefore, based on the extracted aquaculture area, the nutrient exchange flux per day was estimated (in the summer and autumn) for the study area. Additionally, considering the influencing factors, such as the type of substrate, the vertical diffusion rate of each inorganic nutrient was determined as follows (Table XIII and Table XIV).

Finally, we obtained the nutrients produced through aquaculture activities and the nutrients produced from the two different sources. They are listed in Table XV.

It can be seen from Tables XII and XV that excretion was the main source for the introduction of inorganic nutrients in the aquaculture area, which caused heavy eutrophication pressure in the aquaculture area. This indicates that the scale and density of the aquaculture should be controlled, and the seawater environment needs to be monitored regularly in order to lower the potential ecological risks.

VIII. CONCLUSION

The Gouqi Island oyster cage aquaculture area was taken as the test area in this study in order to obtain feasible extraction methods for the aquaculture area in dynamically varying turbid sea area with good performance. A set of rules for different water body methods was proposed in order to achieve the accurate extraction of the aquaculture area. The extraction results were compared with three different conventional classification methods, including maximum likelihood classification, neural network, and SVM. Further verification test is performed for three GF-2 images of aquaculture in uniformly clean water, different types of aquacultures in turbid and same aquaculture area in Gouqi Island however, taken at different time. The concluding remarks are as follows.

The proposed extraction method proposed in this study showed higher precision than the three conventional methods with an acceptable operation cost especially for those aquaculture with obscured properties, such as color, shape, or texture, for the complex water environment with varying turbidity. The reason for this was that our proposed method not only used spectral features in the construction of the feature index and rule set, but also introduced features, such as shape, area, and texture, when segmentation and extraction were performed. The extraction effect for each category of water body with different turbidity could be optimized through the restriction of rules, so the combined overall extraction results achieved better results.

The extracted area of the aquaculture with the object-based extraction methods developed in this study was used to estimate the nutrient loading in this sea area that was induced by the oyster aquaculture. The results indicated that the *N* and *P* loads in the culture area were very high, which results in a large amount of *N* and *P* being recycled by oyster excretion and sediment decomposition. The released nutrients caused huge eutrophication pressure locally. The nutrient output through excretion was much higher than that of the sediment exchange.

The study results demonstrated that our method is able to provide technical support for the aquaculture industry and marine environment management.

REFERENCES

[1] Food and Agriculture Organization of the United Nations, "The State of World Fisheries and Aquaculture 2016: Contributing to the full realization of food and nutrition security," Rome, Italy, 2016.
[2] China National Oceanic Administration, "Bulletin on the state of China's marine eco-environment in 2017," Beijing, China, Mar. 2017.
[3] Y. B. Yang, N. Jiang, L. Q. Ying, and B. Hu, "RS-based dynamic monitoring of lake area and enclosure culture in East Taihu lake," *J. Lake Sci.*, vol. 17, no. 2, pp. 133–138, Jul. 2005.
[4] J. Wang and J. F. Gao, "Extraction culture in Gehu lake based on correspondence analysis," *J. Remote Sens.*, vol. 12, no. 5, pp. 716–723, Sep. 2008.
[5] Y. J. Ma, D. L. Zhao, R. M. Wang, and W. Su, "Offshore aquatic farming areas extraction method based on ASTER data," *Trans. Chin. Soc. Agricultural Eng.*, vol. 26, no. s2, pp. 120–124, Dec. 2010.
[6] S. Jeffrey and E. John, "*Geographic Information Systems: An Introduction*. Englewood Cliffs, NJ, USA: Prentice-Hall, 1990.
[7] A. Voulodimos, N. Doulamis, A. Doulamis, and E. Protopapadakis, "Deep learning for computer vision: A brief review," *Comput. Intell. Neurosci.*, vol. 2018, pp. 1–13, Feb. 2018.
[8] Z. W. Ren and L. D. Wu, "Hyperspectral intrinsic image decomposition based on automatic subspace partitioning," *Laser Optoelectron. Prog.*, vol. 55, no. 10, pp. 398–404, May 2018.
[9] N. Shu and Z. Q. Shen, "Continuous Bayesian network classifier for remote sensing images based on improved Gaussian mixture model," *Remote Sens. Inf.*, no. 2, pp. 18–29, Apr. 2010.
[10] S. Xu, L. H. Xia, H. B. Peng, and X. Li, "Remote sensing extraction of mariculture models based on object-oriented," *Geomatics Spatial Inf. Technol.*, vol. 41, no. 5, pp. 110–112, May 2018.

[11] T. F. Cheng, W. F. Zhou, and W. Fan, "Progress in the methods for extracting aquaculture areas from remote sensing data," *Remote Sens. Land Resour.*, vol. 24, no. 3, pp. 1–5, Sep. 2012.
[12] Y. J. Ma, D. L. Zhao, and R. M. Wang, "Comparative study of the offshore aquatic farming areas extraction method based on ASTER data," *Bull. Surv. Mapping*, vol. 2011, no. 1, pp. 59–63, Jan. 2011.
[13] X. Lu *et al.*, "The identification of porphyra culture area by remote sensing and spatial distribution change and driving factors analysis," *Mar. Sci.*, vol. 42, no. 7, pp. 87–96, Jul. 2018.
[14] Y. LeCun, Y. Bengio, and G. Hinton, "Deep learning," *Nature*, vol. 521, pp. 436–444, May 2015.
[15] H.-J. Yoo, "Deep convolution neural networks in computer vision: A review," *IEIE Trans. Smart Process. Comput.*, vol. 4, no. 1, pp. 35–43, Feb. 2015.
[16] D. S. Liu and X. Fan, "Assessing object-based classification: Advantages and limitations," *Remote Sens. Lett.*, vol. 1, pp. 187–194, Apr. 2010.
[17] R. Pu, S. Landry, and Q. Yu, "Object-based urban detailed land cover classification with high spatial resolution IKONOS imagery," *Int. J. Remote Sens.*, vol. 32, pp. 3285–3308, Jun. 2011.
[18] Y. Zhang and Y. G. Wang, "Remote sensing technology of subwater topography," *Ocean Eng.*, vol. 18, no. 3, pp. 88–91, Aug. 2000.
[19] W. Li, "Research on the object-oriented classification technology of high resolution remote sensing imagery," M.S. thesis, School Surveying Mapping, Jiangsu Normal Univ., Xuzhou, China, 2013.
[20] S. R. Yang, Z. H. Xue, L. Zhang, H. Su, and S. Zhou, "Fusion of hyperspectral and LiDAR data: A case study for refined crop classification in agricultural region of Zhangye Oasis in the middle reaches of Heihe River," *Remote Sens. Land Resour.*, vol. 30, no. 4, pp. 33–40, Dec. 2018.
[21] C. B. Lin and S. Q. Li, "Research progress of water-body automatic extraction methods in Landsat data," *Autom. Technol. Appl.*, vol. 34, no. 2, pp. 1–4, 2015.
[22] X. P. Wu, H. Q. Xu, and Q. L. Jiang, "Cross-comparison of GF-1, GF-2 and Landsat-8 sensor data," *J. Ecology*, vol. 33, no. 11, pp. 3249–3257, 2013.
[23] B. B. Jiang *et al.*, "Using GOCI extracting information of red tide for time-series analysing in East China Sea," *J. Zhejiang Univ. (Sci. Ed.)*, vol. 44, no. 5, pp. 566–583, Sep. 2017.
[24] J. X. Chen, X. Y. Zhang, and G. R. Huang, "Diffuse attenuation coefficient inversion for the Yangtze Estuary and its adjacent sea areas on the GOCI images and application in the preevaluation of airborne laser bathymetry," in *Proc. 8th Int. Conf. Agro-Geoinformat.*, 2019, pp. 1–6.
[25] M. C. Zhang and B. Y. Gou, "Retrieval of suspended sediment concentration in Zhoushan coastal area satellite based on GF-1," *Mar. Develop. Manage.*, vol. 35, no. 1, pp. 126–131, Jan. 2018.
[26] H. S. Zhang, "*The Basic Status of Marine Environmental Resources in Zhejiang Province*. Beijing, China: Ocean Press, 2013.
[27] B. B. Jiang *et al.*, "Retrieving high concentration of suspended based on GOCI: An example of coastal water around Hangzhou Bay, China," *J. Zhejiang Univ. (Sci. Ed.)*, vol. 42, no. 2, pp. 213–220, Mar. 2015.
[28] W. F. Gong, P. Wang, S. Y. Wang, Y. Zhou, and K.-H. Cao, "Methods of water body extraction in boundary river based on GF-2 satellite remote sensing image of high resolution," *J. Eng. Heilongjiang Univ.*, vol. 9, no. 4, pp. 1–7, Dec. 2018.
[29] Y. W. Lu, Q. Z. Li, X. Du, H.-Y. Wang, and J.-L. Liu, "A method of coastal aquaculture area automatic extraction with high spatial resolution images," *Remote Sens. Technol. Appl.*, vol. 30, no. 3, pp. 486–494, Jun. 2015.
[30] B. Cheng, Y. M. Liu, X. N. Liu, G. Wang, and X. Ma, "Research on extraction method of coastal aquaculture areas on high resolution remote sensing image based on multi-features fusion," *Remote Sens. Technol. Appl.*, vol. 33, no. 2, pp. 296–304, Apr. 2018.
[31] H. L. Ge, "Research on class-oriented image segmentation method," Ph.D. dissertation, School Forestry, Beijing Forestry Univ., Beijing, China, 2004.
[32] W. Hanston, L. Kooistra, and P. A. Slim, "Mapping invasive woody species in coastal dunes in the Netherlands: A remote sensing approach using LIDAR and high-resolution aerial photographs," *Appl. Vegetation Sci.*, vol. 15, no. 4, pp. 536–547, Oct. 2012.
[33] Y. Y Sun *et al.*, "Research on object-oriented classification and dynamic monitoring of sea information for marine aquaculture," *Mar. Inf.*, vol. 216, no. 2, pp. 6–11, May 2016.
[34] S. Y. Cheng *et al.*, "Comparisons of supervised classification methods for land cover based on high spatial resolution remote sensing image in Shaliu river basin of Qinghai lake," *Bull. Soil Water Conservation*, vol. 38, no. 5, pp. 261–268, Oct. 2018.
[35] Y. Yan, X. L. Dong, and Y. Li, "The comparative study of remote sensing image supervised classification methods based on ENVI," *Beijing Surv. Mapping*, vol. 3, no. 3, pp. 14–16, Mar. 2011.
[36] K. Sun and T. D. Lu, "Comparison of supervised classification methods in remote sensing image classification," *Jiangxi Sci.*, vol. 35, no. 3, pp. 367–371, Oct. 2017.
[37] Z. B. Wu *et al.*, " Study on the effect of the number of training samples on the accuracy of maximum likelihood supervision classification," *Forest Investigation Des.*, no. 2, pp. 115–117, May 2018.
[38] Y. F Ma *et al.*, "Remote sensing image classification based on artificial neural networks," *Standardization Surv. Mapping*, vol. 34, no. 4, pp. 34–37, Dec. 2018.
[39] L. Yao, "Study of remote sensing image classification based on support vector machines," thesis, School Resource Environment, Shandong Normal Univ., Shandong, China, 2012.
[40] Y. Zhou *et al.*, "Nitrogen and phosphorus excretion and its ecological effect by several bivalves and fouling animals," *Oceanologia Et limnologia Sinica*, vol. 33, no. 4, pp. 424–431, Jul. 2002.
[41] Y. J. Fu, "The growth characteristics of mytilus edulis linnaeu in Gouqi island and its effect on the water quality," M.S. thesis, School Fisheries, Zhejiang Ocean Univ., Zhoushan, China, 2014.

Xiaoyu Zhang was born in Zhejiang, China, in 1972. She received the Ph.D. degree in physical electronics and engineering from the Chinese Academy of Sciences, Shanghai, China, in 2006.

From 1999 to 2006, she was a Lecturer with the Department of Earth Science, Zhejiang University, Hangzhou, China. Since 2007, she has been an Assistant Professor with the College of Earth Science, Zhejiang University. She is the author of two books and more than 50 articles. Her research interests include remote sensing of ocean color with multisatellite data, marine and inland water environment quality and ecological healthy monitor and assessment, and optical properties of water parameters and applications.

Shuchang Ma was born in Lishui, China, in 1997. She received the B.S. degree in natural geography and resources environment from Yunnan University, Kunming, China, in 2019. She is currently working toward the M.S. degree in geological engineering with Zhejiang University, Hangzhou, China.

Her research interests include the algorithms of ocean color retrieval, remote sensing dynamic monitoring and evaluation of estuary, and coastal water quality.

Cheng Su was born in 1985. He received the B.S. degree in geology from Tongji University, Shanghai, China, in 2007, and the Ph.D. degree in earth exploration and information technology from Zhejiang University, Hangzhou, China, in 2012.

From 2012 to 2018, he was an Assistant Professor with the Institute of Spatial Information and Technology, Zhejiang University. He is currently an Associate Professor with the School of Earth Science and the Deputy Director with the Institute of Geography and Spatial Information, Zhejiang University. His research interests include the remote sensing image process, spatial data analysis, and earth big data modeling.

Yongheng Shang was born in Zhengzhou, China, in 1978. He received the B.S. degree in electronic engineering from the University of Surrey, Guildford, U.K., in 2005, and the Ph.D. degree in electronic engineering from the Surrey Space Center, University of Surrey, in 2011.

Between 2007 and 2010, he was a Math Tutor and Laboratory Supervisor with the Faculty of Engineering and Physical Science, University of Surrey. From 2011 to 2013, he was a Postdoc with the School of Aeronautic and Astronautic, and from 2013 to 2019, he was a Lecturer and an Assistant Researcher with the Institute of Advanced Technology, Zhejiang University, Hangzhou, China. Since 2020, he has been an Associate Professor with the Institute of Advanced Technology, Zhejiang University. He is the author of more than 40 articles and 20 inventions. He holds eight patents. His research interests include remote sensing technologies, signal processing, and smart space robotics.

Dr. Shang was a member of the American Association for the Advancement of Science. He was the recipient of the RAS Award, in 2009.

Luming Zhang, biography not available at the time of publication.

Tinggang Wang was born in Huaibei, China, in 1994. He received the B.S. degree in geography national conditions monitoring from Wuhan University, Wuhan, China, in 2016, and the M.S. degree in geological engineering from Zhejiang University, Hangzhou, China, in 2019.

His research interests include the remote sensing image process and the algorithms of ocean color retrieval.

Jianwei Yin was born in Xuzhou, China, in 1974. He received the Ph.D. degree in computer science and engineering from the Zhejiang University, Hangzhou, China, in 2001.

From 2001 to 2003, he was a Lecturer with the School of Computer Science and Technology, Zhejiang University. He has been promoted as an Associate Professor, in 2004 and become a Full Professor, in 2009. Since 2017, he has been the Vice Dean with the School of Computer Science and Technology, Zhejiang University. In 2008, he was with the Georgia Institute of Technology as a Visiting Scholar, and he went to the University of California, Santa Barbara as a Visiting Scholar between 2013 and 2014. He is the author of three books, more than 200 articles, and more than 100 patents. His research interests include service computing, distributed computing, data science, artificial intelligence, and remote sensing data processing and application.

Prof. Yin is an Associate Editor for the IEEE TRANSACTIONS ON SERVICE COMPUTING. He served as a PC Chair for many prestigious international conferences, such as ICDCS2018, ICSOC2018, ICWS2020, CIC, etc. He was a recipient of the second class prizes of the State Science and Technology Award, in 2010, the first class prizes of Science and Technology Awards from the Ministry of Education of the PRC, in 2008, three provincial-level first class prizes of Science and Technology Awards, in 2008, 2009, and 2014, and the Best ICSOC Paper Award, in 2017.